Cell PRESS

SIK2 Is a Centrosome Kinase Required for Bipolar Mitotic Spindle Formation that Provides a Potential Target for Therapy in Ovarian Cancer

Ahmed Ashour Ahmed,[1,4,5,9,*] Zhen Lu,[1] Nicholas B. Jennings,[2] Dariush Etemadmoghadam,[7] Luisa Capalbo,[6] Rodrigo O. Jacamo,[3] Nuno Barbosa-Morais,[8] Xiao-Feng Le,[1] Australian Ovarian Cancer Study Group, Pablo Vivas-Mejia,[1] Gabriel Lopez-Berestein,[1] Geoffrey Grandjean,[1] Geoffrey Bartholomeusz,[1] Warren Liao,[1] Michael Andreeff,[3] David Bowtell,[7] David M. Glover,[6] Anil K. Sood,[2] and Robert C. Bast, Jr.[1,*]

[1]Department of Experimental Therapeutics
[2]Department of Gynecologic Oncology
[3]Department of Stem Cell Transplantation and Cellular Therapy
M.D. Anderson Cancer Center, University of Texas, Houston, TX 77030, USA
[4]Department of Oncology, University of Cambridge, Hutchison/MRC Research Centre, Hills Road, Cambridge CB2 0XZ, UK
[5]Department of Obstetrics and Gynaecology, University of Cambridge, The Rosie Hospital, Robinson Way, Cambridge CB2 0SW, UK
[6]Department of Genetics, University of Cambridge, Downing Street, Cambridge CB2 3EH, UK
[7]Cancer Genomics and Genetics Laboratory, Peter MacCallum Cancer Centre, St Andrew's Place, East Melbourne 8006, Victoria, Australia
[8]Computational Biology Group, Department of Oncology, University of Cambridge, Cancer Research UK Cambridge Research Institute, Li Ka Shing Centre, Cambridge CB2 0RE, UK
[9]Present address: The Nuffield Department of Obstetrics and Gynaecology, University of Oxford, John Radcliffe Hospital, Level 3, Women's Centre, Oxford OX3 9DU, UK
*Correspondence: ahmed.ahmed@obs-gyn.ox.ac.uk (A.A.A.), rbast@mdanderson.org (R.C.B.)
DOI 10.1016/j.ccr.2010.06.018

SUMMARY

Regulators of mitosis have been successfully targeted to enhance response to taxane chemotherapy. Here, we show that the salt inducible kinase 2 (SIK2) localizes at the centrosome, plays a key role in the initiation of mitosis, and regulates the localization of the centrosome linker protein, C-Nap1, through S2392 phosphorylation. Interference with the known SIK2 inhibitor PKA induced SIK2-dependent centrosome splitting in interphase while *SIK2* depletion blocked centrosome separation in mitosis, sensitizing ovarian cancers to paclitaxel in culture and in xenografts. Depletion of *SIK2* also delayed G1/S transition and reduced AKT phosphorylation. Higher expression of *SIK2* significantly correlated with poor survival in patients with high-grade serous ovarian cancers. We believe these data identify SIK2 as a plausible target for therapy in ovarian cancers.

INTRODUCTION

Uncontrolled mitosis is a distinguishing feature of cancer cells that has been effectively exploited for cancer therapy using anti-tubulin drugs such as paclitaxel. The use of primary paclitaxel-based combination chemotherapy increases progression free survival and overall survival in hematological and solid malignancies including ovarian cancer (Martin et al., 2008; McGuire et al.,

1996). Whereas high-grade serous ovarian cancers are known to be highly chemosensitive, a significant proportion of these cancers fail to respond to primary taxane therapy leading to the emergence of resistant disease. There is a pressing need for the discovery of synergistic therapies that may improve ovarian cancer response to taxane-based chemotherapy and overall prognosis. Currently available mechanisms for selective enhancement of taxane response, such as the use of kinesin

Significance

Taxanes stabilize microtubules, inhibit mitosis, induce apoptosis, and produce regression in a fraction of cancers that arise at many sites including the ovary. The anti-tumor activity of taxanes might be increased by concurrently regulating kinases that affect both cell cycle and mitosis. Here we show that SIK2 localizes at the centrosome, phosphorylates the centrosome linker protein C-Nap1 and plays a key role in regulating the onset of mitosis. *SIK2* depletion resulted in profound synergy with paclitaxel in inducing cytotoxicity, whereas higher expression in ovarian cancers correlated with poor prognosis. Independent of its antimitotic role, SIK2 targeting resulted in decreased G1/S transition and low AKT phosphorylation. Thus, SIK2 provides a multimodal therapeutic target in a subset of ovarian cancers.
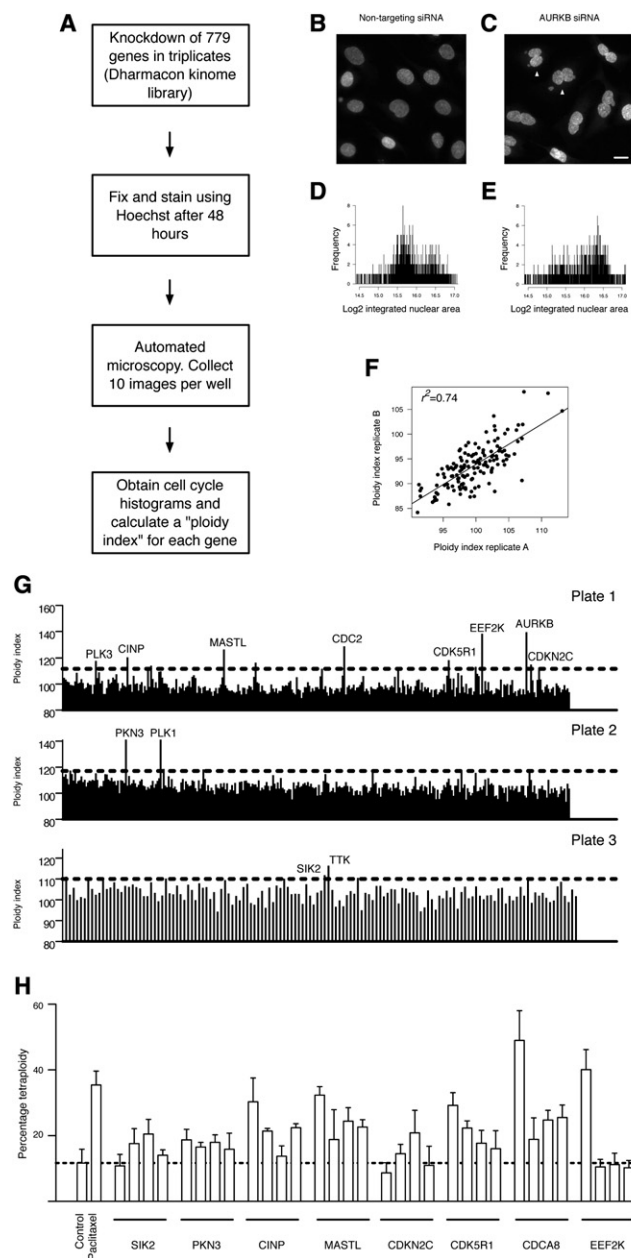
Figure 1. A Kinome siRNA Screen Identifies Regulators of G2/M Progression in Ovarian Cancer

(A) A schematic presentation of the siRNA kinome screen.

(B–H) Each of the 779 genes included in the screen was targeted using pools of four individual siRNAs. These pools were divided into three plates (320 pools for plates 1 and 2 and 139 pools in plate 3). Three replicates were used for each plate, and ten images were obtained per well. Integrated nuclear intensity (INI) values for individual cells, defined as the nuclear area multiplied by its mean pixel intensity, were extracted from 32,400 images, including a total of 1,946,532 cells. The calculation of the percentage shift of the median integrated nuclear intensity value (ploidy index) is explained in (B–E). Images were obtained 48 hr after transfection with (B) nontargeting siRNAs or (C) a pool of siRNAs targeting AURKB. Arrow heads in (C) point to examples of fused nuclei. Scale bar represents 10 μm. The INI values were used to generate cell-cycle histograms after (D) nontargeting siRNA transfection or (E) AURKB siRNA transfection. Note the shift to the right of the log2 INI values in (E) as a consequence of tetraploidy. The ploidy index (PInd) was obtained as the

motor inhibitors or the inhibition of mitotic exit, are focused on targeting cancer cells only in mitosis (Huang et al., 2009; Mayer et al., 1999). Although such strategies have shown clinical promise, overall tumor response rates have been limited (Blagden et al., 2008; Gautschi et al., 2008; Lin et al., 2008; Strebhardt and Ullrich, 2006). Novel therapeutic targets that augment taxane effects in inhibiting mitosis while providing taxane- and mitosis-independent mechanisms of cancer cell death are needed to improve clinical chemotherapy response. In this work we conducted an siRNA-based screen to identify modulators of mitotic progression that may influence clinical paclitaxel response.

RESULTS

A High Content siRNA Kinome Screen Identifies Cell-Cycle Regulators of Ovarian Cancer Cells

Recent evidence suggests that delayed mitotic progression or the inhibition of mitotic exit are key predictors of cell death either with or without taxane treatment (Bekier et al., 2009; Huang et al., 2009). To identify regulators of mitotic progression in ovarian cancer cells that may modulate taxane response, we used a three-step approach: (1) we screened 779 pools of siRNAs (Dharmacon kinome library) targeting individual genes to identify potential regulators of the G2 or the M phases (G2/M) of the cell cycle; (2) several hits were selected for further validation using individual siRNAs that made up the pool used in the primary screen; and (3) time-lapse microscopy was used to identify specific regulators of mitotic progression that were then tested for synergistic interactions with paclitaxel.

The primary screen used automated image acquisition and morphometric analysis of fixed cells in 384-well plates (high content analysis, Figure 1A) to measure single-cell DNA content after siRNA treatment. The integrated nuclear intensity values (defined as the nuclear area multiplied by its mean pixel intensity) were calculated as a measure for DNA content and used to generate cell-cycle histograms after the knockdown (KD) of each of the 779 genes included in the screen. The percentage of shift of the median integrated nuclear intensity value after a gene KD compared to that after transfection using nontargeting siRNA was calculated and termed the ploidy index (Figures 1B–1E and Table S1 available online). Genes that on KD induced a percentage shift (ploidy index) that was above the median and 2 standard deviations (SD) of all genes in a plate were identified as positive hits for further validation (Figure 1G and Table S2). There was a high correlation between the ploidy indices across triplicate plates (median correlation coefficient = 0.74) and a mean coefficient of repeatability for all genes tested of 0.1, indicating high data precision in the screen (Figure 1F, Figure S1A,

percentage of the median INI after gene knockdown normalized to the median INI after control transfection. (F) An example of the correlation between the ploidy indices of two replicate plates in the screen. In (G), the cutoff PInds for each plate and examples of the identified hits are shown. (H) The percentage of the tetraploid cells in relation to the total number of cells after either paclitaxel treatment, as a positive control for tetraploidy, or knockdown of genes using four independent siRNAs. The mean ± SD of triplicates is presented.

See also Figure S1 and Tables S1–S3.

and Table S1). The identified hits included many genes that have been previously shown to regulate G2 or M phases of cell-cycle progression such as cyclin dependent kinase 1 (*CDC2*) and polo kinase 1 (*PLK1*) (Table S2). The magnitude of ploidy shift varied according to the mechanism of G2/M regulation by a gene rather than the biological importance. For example, depletion of Aurora kinase B (*AURKB*) resulted in cytokinesis failure and a profound increase in the ploidy index. In contrast, depletion of the centrosome kinase phosphotyrosine picked threonine kinase 1 (*MPS1*, also called *TTK*) resulted in a modest increase in ploidy that presumably reflects delayed mitotic transition (Tables S1–S3).

Among the identified hits, seven were selected for further validation based on their potential novelty (Figure 1H). To exclude off-target effects, we used four individual siRNAs that made up the siRNA pool that was used in the primary screen to KD each gene and compared the percentage of tetraploid cells after genetic KD with the percentage after transfection with a nontargeting siRNA control. As a positive control for tetraploidy we used (1) paclitaxel treated nontransfected cells and (2) KD of the chromosome passenger protein Borealin (*CDCA8*), which plays a critical role in cytokinesis. Six of the seven genes were validated with at least 2 independent siRNAs, which resulted in a significant increase in tetraploidy (p < 0.05, Wilcoxon test, Figure 1H). Only one of the four siRNAs targeting the eukaryotic elongation factor-2 kinase (*EEF2K*) resulted in increased tetraploidy indicating an off-target effect. Interestingly, this siRNA had a perfect sequence match to *EEF2K* and also 70% sequence match to Borealin.

The six validated targets may be involved in the regulation of G2, mitosis or both. To determine specific regulators of mitosis we used bright field microscopy and time lapse imaging to identify targets that lead to delayed mitotic progression. To demonstrate the opposite effect, we used KD of the mitotic checkpoint protein BUBR1 and, as expected, this resulted in rapid mitotic progression (mean = 20 min after KD of *BUBR1* compared to 58 min in controls, n = 10, p < 0.01; Movies S1 and S2). In contrast, depletion of *SIK2*, cyclin dependent kinase 2 interacting protein (*CINP*) or CDK5 regulatory subunit 1 (*CDK5R1*) resulted in a significant delay in mitotic progression followed by mitotic exit without cell division (Movie S3 and data not shown).

The finding that SIK2 may play a role in regulating mitosis was intriguing because its established functional role has been in the regulation of cellular metabolism but not the cell cycle (Dentin et al., 2007; Katoh et al., 2004; Screaton et al., 2004). We have previously shown that KD of the *Drosophila* orthologs of serine/threonine kinase 11 (*STK11*, also called *LKB1*), a known SIK2 kinase, and *SIK3*, an immediate family member of SIK2 results in severe mitotic abnormalities (Bettencourt-Dias et al., 2004). We, therefore, selected *SIK2* for further validation. Time-lapse photography showed that loss of *SIK2* resulted in a dramatic increase in the mean mitotic progression time (62 min in control cells transfected with nontargeting siRNA versus 133, 209, and 172 min after *SIK2* KD using three siRNAs, p < 0.001, one-way ANOVA and Tukey's multiple comparisons test) (Figures 2A–2D). Importantly many of the *SIK2* depleted cells either did not exit mitosis during the time of recording, ruptured or failed to undergo cytokinesis (Movie S3 and data not shown).
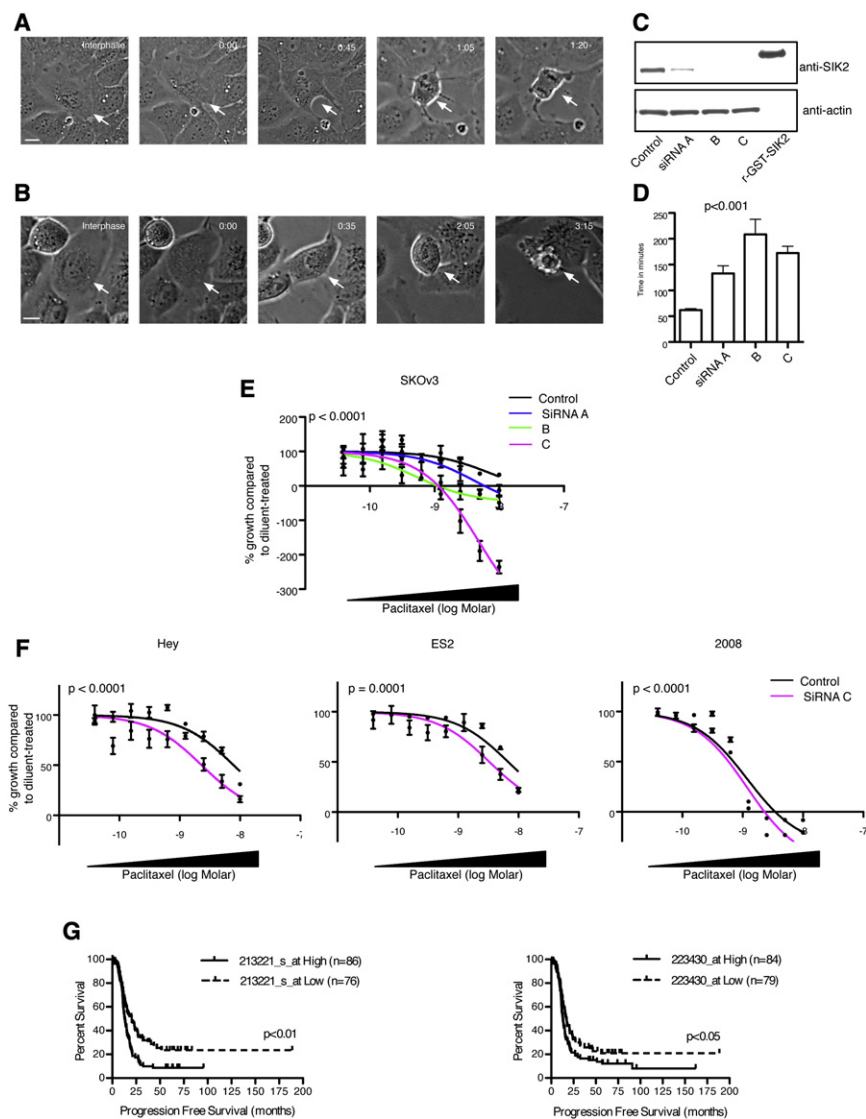
Depletion of *SIK2* Sensitizes Ovarian Cancers to Paclitaxel

As depletion of *SIK2* resulted in protracted mitotic progression time, we tested the hypothesis that this may sensitize ovarian cancer cells to paclitaxel. Transfection with *SIK2* siRNA decreased the dose of paclitaxel required to reduce cancer cell growth by 50% (GI 50) from 4.8 nM (95% confidence interval [CI]: 2.7–8.4 nM) in control-transfected cells to 1.4 nM (95% CI: 0.6–3.2 nM), 0.17 nM (95% CI: 0.05–0.6 nM), or 0.36 nM (95% CI: 0.01–0.1 nM) for *SIK2* siRNAs A, B, and C, respectively (Figure 2E). Importantly, this effect was not cell specific as *SIK2* KD significantly decreased paclitaxel GI 50 in Hey cells (from 7.8 nM for control siRNA to 2.3 nM for *SIK2* siRNA), ES2 cells (from 6.7 nM for control siRNA to 3.3 nM for *SIK2* siRNA) and 2008 cells (from 0.67 nM for control siRNA to 0.47 nM for *SIK2* siRNA) (Figure 2F), indicating that selective depletion of *SIK2* is sufficient to sensitize ovarian cancer cells to paclitaxel in vitro.

To test the biological significance of *SIK2* in ovarian cancer we first examined its expression pattern in 59 ovarian cancers and nine pools of normal ovarian surface epithelial cells using quantitative PCR. The range of expression of *SIK2* was narrow suggesting that a large number of cases was required to identify a correlation between *SIK2* expression and clinical outcome (data not shown). The importance of *SIK2* in regulating mitosis and paclitaxel response was supported by the analysis of *SIK2* expression in 229 patients with high-grade serous (HGS) ovarian cancers in a population-based study (Tothill et al., 2008). Higher expression of *SIK2* significantly increased the hazard of cancer progression after taxane-based chemotherapy using the two independent affymetrix microarray probe sets that were found to accurately represent *SIK2* expression (Figure 2G and Figure S2A). These results were validated using quantitative PCR (Figure S2B). In addition, the level of *SIK2* microarray expression in paclitaxel or carboplatin resistant ovarian cancers was compared to that in paclitaxel or carboplatin responders in a prospective randomized clinical trial in which patients with primary ovarian cancer were treated initially with either single agent paclitaxel or single agent carboplatin for three cycles (Ahmed et al., 2007). *SIK2* expression was significantly higher in paclitaxel resistant compared to paclitaxel-sensitive cancers (p = 0.028, one-sided t test, n = 20; Figure S2C). In contrast, no significant difference was found in *SIK2* expression between carboplatin resistant or carboplatin sensitive cancers (p = 0.7, one-sided t test, n = 15; Figure S2C). All together these data support an important role of *SIK2* in the regulation of mitosis and taxane response in cell culture and in ovarian cancer patients.

SIK2 Localizes at the Centrosome

To investigate a possible physical association between SIK2 and the mitotic spindle, we examined the subcellular localization of SIK2 using immunofluorescence (IF). As previously described, endogenous SIK2 was observed in the cytoplasm (Katoh et al., 2004). In addition, SIK2 colocalized with γ-tubulin in the centrosomes of 70% of cells in interphase and in all cells in mitosis and coimmunoprecipitated with γ-tubulin (Figure 3A and Figure S3A). Preincubation of the SIK2 antibody with recombinant SIK2 protein, but not with control proteins (BSA

Figure 2. Depletion of *SIK2* Delays Mitotic Progression and Sensitizes Ovarian Cancer Cells to Paclitaxel

(A–D) SKOv3 cells were transfected with either (A) nontargeting siRNA or (B) SIK2 siRNA for 48 hr then monitored for 16 hr (one image every 5 min) using bright field phase-contrast microscopy. The time interval from nuclear envelope breakdown (0:00 in A and B) to anaphase onset (01:20 in control cells) was estimated. Arrows point to the cell under study. Time is shown as hr:min. Scale bar represents 10 μm. In (C), western blot confirmation of knockdown of *SIK2* using three independent siRNAs compared to nontargeting siRNA control is shown. r-GST-SIK2; recombinant GST-tagged SIK2 was used on the same western blot to confirm the antibody specificity. (D) The mean ± SEM of the mitotic transition time (obtained as in A and B) is presented after control and *SIK2* siRNA transfections.

(E) SKOv3 cells (5000 cells per well) were reverse transfected in 96-well plates using either nontargeting controls or *SIK2* siRNAs (A), (B), and (C) for 24 hr and cells were then either (a) fixed and stained using crystal violet to estimate the number of cells on the day of paclitaxel treatment (day 0); or (b) treated with either diluent or paclitaxel at 9 different concentrations. The latter group of cells was fixed and stained 72 hr after drug treatment. Growth of cells from day 0 to day 3 was estimated and the percentage paclitaxel-induced growth inhibition for each siRNA in relation to diluents-treated cells transfected with the same siRNA was calculated and a least-squares fit was obtained to estimate the GI 50 as described in Experimental Procedures (Monks et al., 1991). Shown is the mean ± SEM from three replicates per concentration.

(F) The effect of depletion of *SIK2* using siRNA C on paclitaxel response in three cell lines is shown. The experiment was conducted as in (E). Shown is the mean ± SEM from six replicates per concentration. Also shown is the p value for the comparison between the GI 50 in cells transfected with nontargeting siRNA control versus cells transfected with *SIK2* siRNA.

(G) Microarray expression data for two probe sets representing *SIK2* were used to generate Kaplan-Meier survival curves for high expressing (defined as cancers with values above the median + (0.5 × median absolute deviation [MAD]) or low expressing (below the median − (0.5 × MAD) for 229 high-grade serous (HGS) ovarian cancers.
See also Figure S2 and Movies S1–S3.

or recombinant histone H1), abolished the centrosome signal of SIK2 on IF (Figure S3B). Further confirmation of specificity was achieved by showing that KD of *SIK2* resulted in a significant decrease in the percentage of cells with detectable SIK2 in the centrosome using immunofluorescence (p < 0.001, t test; Figure S3C). The expression of SIK2 was predominantly pericentriolar as evidenced by immunostaining of HeLa cells that stably expressed GFP-tagged centrin (Figure S3D) and was independent of microtubules because it colocalized with γ-tubulin after nocodazole treatment (data not shown). The observation that endogenous SIK2 localized at centrosomes was further supported by showing that exogenous myc/flag-tagged SIK2 localized to the centrosomes of 50% of the cells examined (Figure 3B). In addition, differential centrosome localization was also

observed after transfection using the untagged version of the *SIK2* plasmid and detection using anti-SIK2 antibody (p < 0.001, paired t test; Figures S3E–H). All together, these results confirm that a pool of SIK2 localizes at the centrosome.

SIK2 Induces Centrosome Splitting
We next tested the functional role of SIK2 in the centrosomes. Examination of the centrosomes in interphase cells transfected with a myc/flag-*SIK2* expression construct revealed a significant increase in the percentage of myc-positive cells with centrosome splitting (CS) compared to the percentage in myc-negative cells or cells transfected with empty vectors (21.3, 5, and 3.9, respectively; p < 0.001, one-way ANOVA; Figures 4A–4C). This effect was not due to failure of re-engagement after
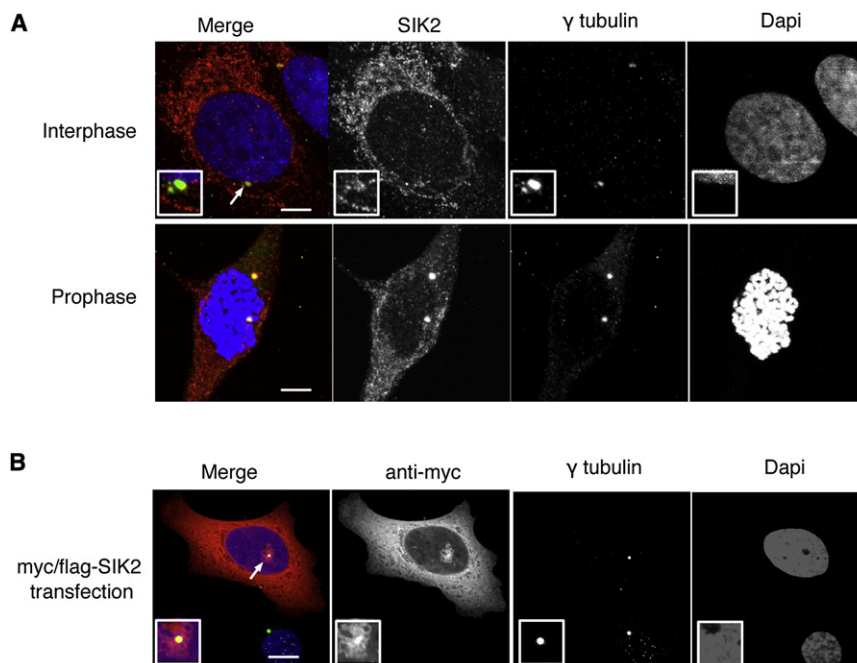
Figure 3. SIK2 Localizes at the Centrosome

(A) SKOv3 cells were fixed and stained for immunofluorescence (IF) using the indicated antibodies to show the colocalization between SIK2 and γ-tubulin.

(B) The colocalization of ectopically expressed myc-tagged *SIK2* with γ-tubulin in SKOv3 cells is shown. Also note the pericentrosomal expression of SIK2. Scale bar represents 5 μm. See also Figure S3.

disengagement that is known to occur in late mitosis to license for centriole duplication (Tsou and Stearns, 2006) as in SKOv3 cells disengaging centrioles only separate by submicrometer distances (Figures S4A–S4G). SIK2-induced CS was dependent on its kinase activity because overexpression of a kinase-inactive SIK2 mutant (SIK2_mt; K49M) (Katoh et al., 2006) did not result in an increase in the percentage of cells with CS (Figures 4B and 4C). The effect of wild-type SIK2 in inducing CS was similar to the reported phenotype that is observed after the overexpression of NEK2 but less in magnitude (3.9% in control cells versus 21.3% in SIK2-positive cells and 50.9% in NEK2-positive cells, p < 0.001; Figures 4B and 4C). Similar results were observed in the osteosarcoma cell line U2OS, a cell line that is commonly used to study this phenotype (4, 29, and 55 for cells transfected with empty vector, SIK2-myc/flag, and NEK2-myc/flag, respectively; p < 0.001, one-way ANOVA; Figure 4C). As the metabolic function of SIK2 is activated after LKB1-induced phosphorylation, we tested the effect of coexpression of SIK2 and LKB1 on CS. LKB1 did not increase the percentage of cells with CS above what is already achieved by SIK2 alone (Figure S4H). This implies that the activity of SIK2 in inducing centrosome splitting is independent of LKB1.

We next took an unbiased approach to identify possible targets for SIK2 phosphorylation in the centrosome. Searching the Swiss-PROT database for human proteins that contains the previously identified putative SIK2 phosphorylation consensus sequence LX[HKR]S/TXSXXXL (Screaton et al., 2004), identified the peptide LHHSLSHSLL in the carboxy-terminal domain (amino acids: 2387–2396) of the centrosome protein CEP250 (also called C-Nap1) as a putative phosphorylation site. C-Nap1 is thought to be one of the key proteins that are required for centrosome cohesion in interphase and its centrosome localization is predominantly regulated by phosphorylation

(Fry et al., 1998a; Mayor et al., 2002). Importantly, phosphorylation of the carboxy-terminal part of C-Nap1 by ectopically expressed NEK2 results in premature exit of C-Nap1 from the centrosome and CS (Fry et al., 1998a, 1998b; Mayor et al., 2002). Recombinant SIK2 directly phosphorylated a 15 amino-acid peptide derived from C-Nap1 that contained the putative SIK2 phosphorylation site at the underlined serine amino acids (LAGLHHSL<u>S</u>H<u>S</u>LLAV) in vitro as shown by liquid chromatography-mass spectrometry (LC-MS), data not shown. In addition, SIK2 catalyzed the incorporation of radioactive γ-^{32}p-ATP into recombinant GST-tagged carboxy-terminal C-Nap1 (GST-C-Nap1-ct, aa; 1982–2442; 461 amino acids), but not GST alone (Figure 4D). Remarkably, LC-MS confirmed that the predominant serine phosphorylation site of the recombinant carboxy-terminal domain of C-Nap1 is S2392 at the predicted consensus phosphorylation sequence and to a lesser extent S2394 (LHHSL<u>S</u>HSLL). Importantly, SIK2 phosphorylation of carboxy-terminal C-Nap1 appeared highly specific as the peptide LHH<u>S</u>LSHSLL was the predominant site of serine phosphorylation in addition to a second site (S2234) at the fifth potential coiled coil region of C-Nap1 (Figure 4E). We next expressed a protein A-tagged version of the carboxy-terminal domain of C-Nap1 in 293-T cells, which are known for their high transfection efficiency. Immunoprecipitation using rabbit IgG-coated beads of protein A-tagged carboxy-terminal C-Nap1 but not protein A alone coprecipitated endogenous SIK2 (Figure 4F) indicating that direct binding between SIK2 and exogenously expressed carboxy-terminal part of C-Nap1 occurs in cells. In addition, endogenous SIK2 partially colocalized with ectopically expressed C-Nap1 in the centrosome of SKOv3 cells (Figure S4I). Co-expression of full length C-Nap1 with the kinase active SIK2 in 293-T cells resulted in the phosphorylation of C-Nap1 as detected by C-Nap1 immunoprecipitation followed by probing using anti-phosphoserine antibody. In contrast expression of the kinase mutant SIK2 did not result in phosphorylation of the coexpressed C-Nap1 (Figure 4G). We next investigated whether SIK2 displaces C-Nap1 from the centrosomes. IF confirmed the localization of endogenous C-Nap1 at the centrosomes of ovarian cancer cells and, in addition, showed that there was variability in the centrosome expression level (Figure S4J). Knockdown of *C-Nap1* resulted in a 10-fold increase in SKOv3 cells with centrosome splitting (Figure S4K).
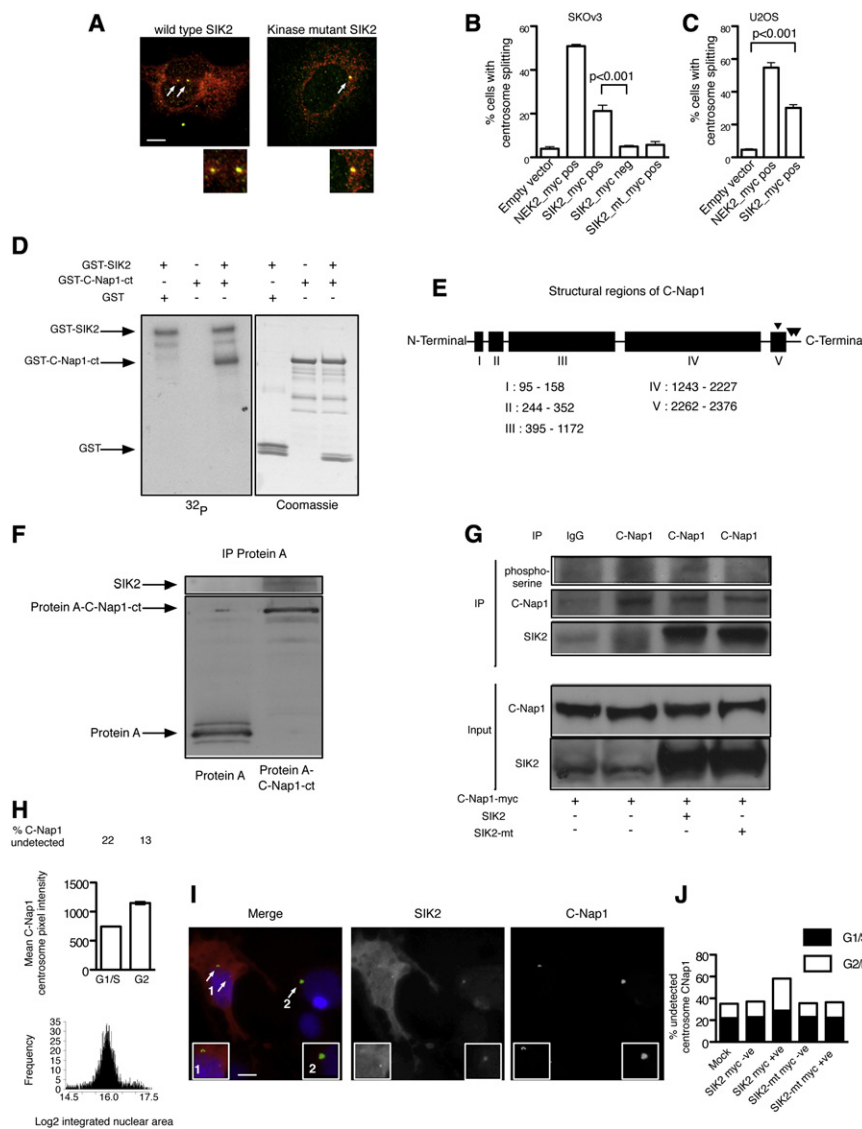
Figure 4. Overexpression of SIK2 Induces Centrosome Splitting through Phosphorylation of C-Nap1

(A) SKOv3 cells were transfected with myc/flag-tagged wild-type *SIK2* or myc/flag-tagged kinase mutant *SIK2* (SIK2_mt) plasmid for 24 hr then cells were fixed and stained using anti-myc antibody (red), and anti-γ-tubulin antibody (green). Arrows show an example of CS (intercentrosome distance > 2 μm) after *SIK2* transfection.

(B and C) Mean ± SEM of the percentage of cells with CS 24 hr after transfection using the indicated plasmids. Overexpression of NEK2, which is known to induce CS, was used as a positive control in this experiment. Experiments were performed at least in triplicates. Scale bar represents 5 μm.

(D) In vitro kinase assays were performed in the presence of either γ-^{32}P-ATP followed by autoradiography (left), or ATP alone followed by Coomassie staining (right). The bands representing GST-C-Nap1-ct were cut and subjected to LC-MS analysis for protein identification and to detect sites of phosphorylation.

(E) A diagram showing the potential five coiled coil domains of C-Nap1 as predicted in the Uniport data base and the serine phosphorylation sites detected by LC-MS at amino acids S2234, S2392, and S2394.

(F) Either Protein A alone or Protein A-tagged C-Nap1-ct were transiently expressed in 293-T cells then immunoprecipitated using Rabbit IgG coated beads followed by elution and separation of the precipitates using SDS-PAGE and immunoblotting using anti-SIK2 antibody.

(G) 293T cells were transfected with the indicated plasmids for 24 hr, then lysates were collected and immunoprecipitation (IP) performed using the indicated antibodies. Immunoprecipitates were resolved by electrophoresis as described in methods then probed with pan anti-phosphoserine antibody initially then anti-C-Nap1 antibody using the same membrane. Also shown is the immunoblot result for SIK2 performed on the same membrane.

(H) Cells were cultured in 384-well plates overnight then fixed and stained using Hoechst nuclear stain and anti-C-Nap1 antibody. Shown is the automated analysis of 4000 cells over 10 replicate wells (as described in Supplemental Experimental Procedures) to identify cell-cycle histograms, mean centrosome intensity value for C-Nap1 ± SEM and the percentage of cells with undetectable C-Nap1 in the centrosomes. Mitotic cells were manually excluded from the analysis.

(I) Cells were transfected with *SIK2* expressing construct for 24 hr then fixed and stained using the indicated antibodies. Note the lower C-Nap1 intensity in the centrosomes of (1) *SIK2*-transfected cell compared to (2) untransfected cell in the same field. Scale bar represents 5 μm. Arrows point to magnified centrosome in the inset.

(J) Shown is the percentage of cells with undetectable C-Nap1 centrosome signal per cell-cycle stage after transfection using the indicated plasmids.
See also Figure S4.

High content analysis of C-Nap1 in untransfected cells showed that its centrosome localization significantly increases in G2 compared to G1/S (p < 0.001, t test; Figure 4H). In addition, the percentage of cells in which the centrosome expression of C-Nap1 was below the automated threshold of detection decreased from 22% in G1/S to 13% in G2. We next examined the effect of *SIK2* transfection on the centrosome localization of C-Nap1 (Figure 4I). *SIK2* transfection resulted in a modest but significant increase of the percentage of cells with undetectable C-Nap1 signal in G1 (22% in SIK2 negative, 27.2% in SIK2 positive, p < 0.001, χ^2 test, n = 3376; Figure 4J). However, in G2, SIK2 expression resulted in a greater magnitude of C-Nap1

displacement (14.5% in SIK2 negative cells to 29.4% in SIK2 positive cells; p = 0.004; χ^2 test, n = 340; Figure 4J). In contrast, expression of a kinase inactive SIK2 did not increase the percentage of cells with undetectable C-Nap1 signal in G1/S or in G2 (Figure 4J). These results implicate C-Nap1 as a putative downstream target for SIK2 at the centrosome.

SIK2 Is Required for Centrosome Separation in Mitosis

As ectopic expression of SIK2 resulted in CS, we tested the hypothesis that endogenous SIK2 was required for centrosome separation in mitosis. Interestingly, in interphase, depletion of *SIK2* resulted in uncoupling of the centrosomes from the nucleus

(Figures S5A and S5B). Importantly, cotransfection of SKOv3 cells with siRNA targeting the 3′UTR of *SIK2* and a construct expressing the open reading frame of *SIK2* completely rescued this phenotype (Figure S5C). Inducing a wound in a confluent monolayer of SKOv3 cells after control siRNA transfection oriented the centrosomes toward the leading edge of the cell. In contrast, cells depleted from *SIK2* failed to orient their centrosomes toward the leading edge in spite of the formation of lamellipodia (Figures S5D and S5E). These results further support the notion of a centrosome-specific function of SIK2. In mitosis, depletion of *SIK2* resulted in the accumulation of cells in prometaphase within 48 hr of transfection (p < 0.01, t test; Figures 5A and 5B). Importantly, this mitotic defect was not because of depletion of energy reserves as knockdown of *SIK2* did not decrease cellular ATP content (Figure S5F). There was a significant increase in the ratio of prometaphase to metaphase cells after *SIK2* KD (2.1 in controls and 8.3 after *SIK2* KD; Figure 5C). These results were confirmed in the U2OS osteosarcoma cell line (Figure 5D). The block in prometaphase was due to failure of *SIK2*-depleted cells to form bipolar mitotic cells (p < 0.001, one-way ANOVA; Figures 5A and 5E). Importantly, the role of SIK2 in regulating centrosome separation in mitosis was evolutionarily conserved, as depletion of the ortholog of SIK2 in *Drosophila* (CG4290) in DMEL cells resulted in a significant increase in mitotic cells with defects in centrosome separation (p < 0.01, t test; Figures 5F and 5G). Thus, SIK2 is required for appropriate centrosome positioning in interphase and for centrosome separation in mitosis.

PRKAR2A Inhibits SIK2 in the Centrosome

We next investigated the mechanisms regulating SIK2 activity in the centrosome. The metabolic function of SIK2 in the cytoplasm is under inhibitory control by PKA (Katoh et al., 2004). Interestingly, the regulatory subunit of PKA, PRKAR2A, is tethered at the centrosome and the pericentriolar region of interphase cells by the anchoring protein AKAP450 (Carlson et al., 2001; Landsverk et al., 2001). In mitosis, CDC2 phosphorylates PRKAR2A resulting in its displacement from the centrosome (Carlson et al., 2001). Consistent with previous observations, we found that PRKAR2A localized to the centrosomes of SKOv3 cells in interphase. In addition, PRKAR2A disappeared from the centrosome early in prophase and this coincided with centrosome separation and a significant increase in the centrosome level of SIK2 and γ-tubulin (p < 0.001, one-way ANOVA; Figures S6A–F).

The centrosome localization of PRKAR2A was required for maintaining centrosome pairing because its depletion in SKOv3 cells resulted in 11.6-fold increase in interphase cells with centrosome splitting compared to control siRNA transfected cells (9.3% and 0.8% respectively; p < 0.001, t test; Figure S6G). To target the centrosome localization of PRKAR2A without interfering with its cytoplasmic level we depleted *AKAP450* in SKOv3 cells (Figure 6A). This depletion abolished the centrosome localization of PRKAR2A but not that of SIK2 (Figure S6H) and resulted in a significant increase in cells with centrosome splitting (CS) (10.8% in *AKAP450* depleted cells versus 1.3% in controls; p < 0.001, one-way ANOVA; Figure 6B). Similar results were obtained using two other *AKAP450* siRNAs, not shown, Importantly, the increase in CS was dependent on SIK2 because cotransfection of SKOv3 cells with siRNAs targeting *SIK2* and *AKAP450* rescued the phenotype (Figure 6B). Thus PRKAR2A is required for preventing *SIK2* from inducing CS in interphase and may play a key role in regulating the appropriate timing of centrosome separation early in mitosis.

SIK2 Is Required for AKT Phosphorylation and Growth of Ovarian Cancer Cells

We next investigated the effect of *SIK2* depletion on cancer cell growth independent from paclitaxel. Depletion of *SIK2* in the ovarian carcinoma cell lines SKOv3, ES2, and Hey resulted in a significant decrease in cancer cell proliferation (Figure 7A, p < 0.001, t test). To investigate the mechanism of suppression of proliferation we tested the effect of depletion of *SIK2* on the cell cycle with or without synchronization. Cell-cycle analysis using flow cytometry of nonsynchronized population of SKOv3 cells after depletion of *SIK2* confirmed the accumulation of tetraploid cells (Figure 7B). However, synchronization of cells in G2/M using paclitaxel treatment after *SIK2* depletion showed that a significant proportion of cells were delayed in G1 (Figure 7B) and failed to enter mitosis as indicated by the significant decrease in mitotic index after paclitaxel treatment (p < 0.001, one-way ANOVA; Figure 7C). These data indicated that loss of SIK2 results in defective G1/S transition in addition to delayed mitotic progression and that both may contribute to suppression of ovarian cancer cell proliferation. To investigate the molecular profile underlying delayed G1/S transition we investigated the effect of *SIK2* depletion on the expression of 139 proteins using reverse phase protein arrays. Depletion of SIK2 resulted in a significant decrease in AKT phosphorylation at amino acid 473 without significantly influencing total AKT expression (Figure 7D). We next examined the effect of SIK2 depletion using three independent siRNAs in three ovarian cancer cell lines on the of expression of 139 proteins and correlated this with cancer cell growth for the cell lines tested, nine expression values for each protein correlated with nine growth proliferation values (Figure 7E and Table S4). Decreased phosphorylation of AKT after *SIK2* depletion resulted in the highest direct correlation with suppression of ovarian cancer cell growth (Pearson's correlation coefficient = 0.83, p = 0.006; Figure 7F). In contrast, depletion of SIK2 resulted in increased LKB1 expression and this significantly correlated with suppression of ovarian cancer cell growth, i.e., a strong negative correlation (Pearson's correlation coefficient = −0.82, p = 0.007).

Loss of *SIK2* Sensitizes Ovarian Cancer to Paclitaxel In Vivo

Based on the above findings, we proposed that depletion of *SIK2* interferes with G1/S progression leading to apparent early resistance to paclitaxel-induced apoptosis due to decreased paclitaxel-induced mitotic arrest (Figure 7C and Figure S7). We hypothesized that cells escaping from G1/S after *SIK2* depletion fail to undergo centrosome separation and that this leads to sensitization to paclitaxel-induced cytotoxicity. To test this hypothesis we used two orthotopic models of ovarian cancer metastasis (SKOv3ip and HeyA8 cancer cells) and in vivo *SIK2* KD using neutral nanoliposomal (DOPC) delivery of siRNA (Figures 8A and 8B). As expected, depletion of *SIK2* resulted in a significant decrease in the mitotic index 24 hr after paclitaxel treatment (p < 0.001, t test, Figures 8C and 8D). However,
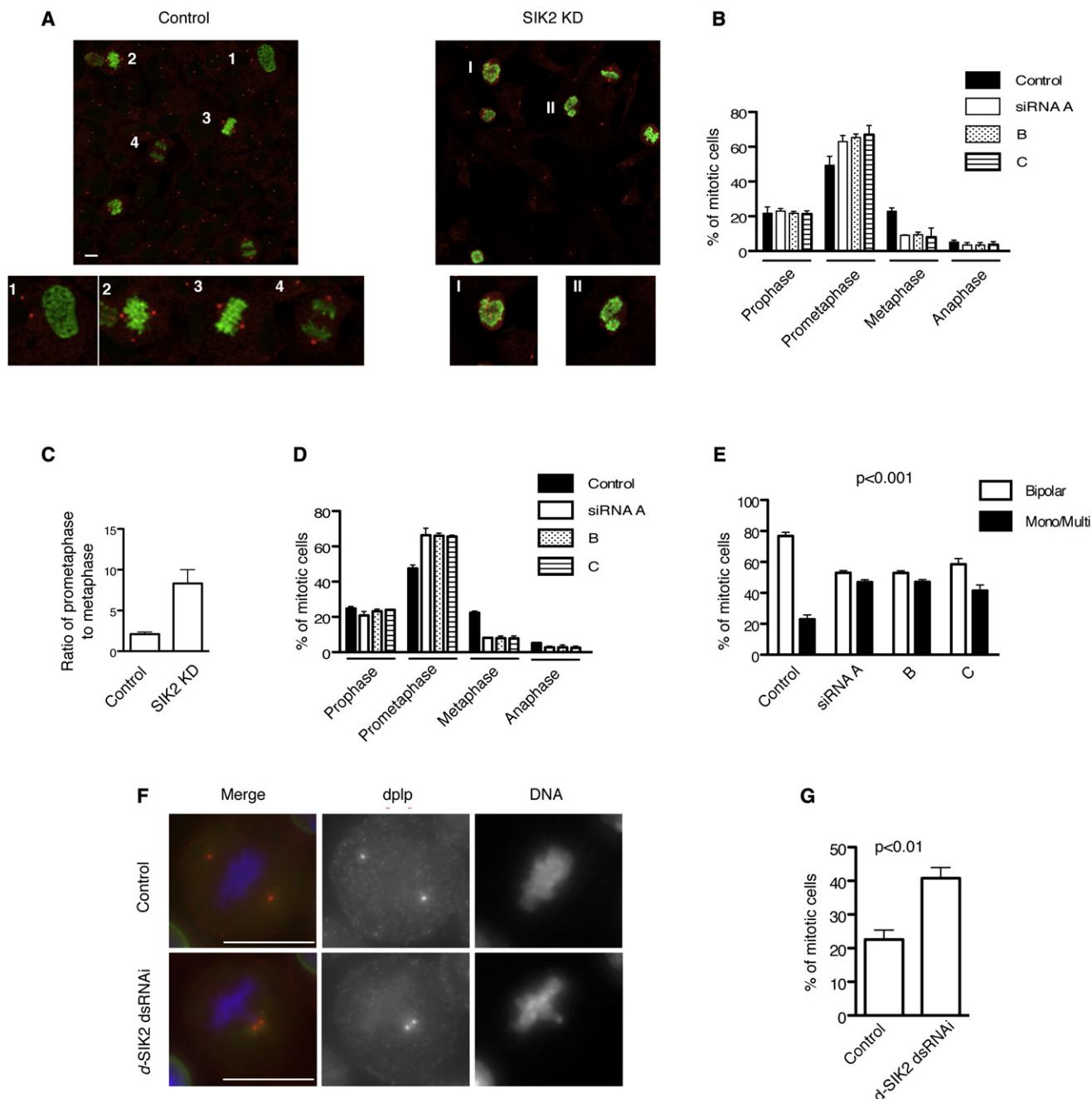
Figure 5. SIK2 Is Required for Centrosome Separation in Mitosis

(A–E) Cancer cells were transfected with siRNAs for 48 hr as indicated then fixed and stained. In (A) and (B), SKOv3 cells were stained using anti-γ-tubulin (red) and anti-phosphohistone H3 (green) to reveal the centosome position in mitosis in relation to chromosomes. Note the presence of examples of different mitosis phases in control cells (1–4: prophase, prometaphase, metaphase, and anaphase, respectively) compared to the predominance of prometaphase cells after *SIK2* KD. Also shown are examples of multipolar (I) and monopolar (II) centrosome positioning after *SIK2* KD. Bar plots in (B) and (D) represent the mean ± SD of the percentages of cells at different stages of mitosis. Bar plots in (C) represent the mean prometaphase/metaphase ratio ± SD.

(F and G) DMEL *Drosophila* cells were transfected using nontargeting control double-stranded RNA (dsRNA) or dsRNAs targeting the *Drosophila* ortholog of *SIK2*. Examples of mitotic cells with failed centrosome separation are presented in (F). In (G), the mean ± SD of mitotic cells with failed centrosome separation from three independent experiments is shown. Scale bars represent 10 μm.

See also Figure S5.

SIK2 KD resulted in a significant increase in monopolar mitotic cells (p < 0.001, Figures 8E and 8F) and a significant decrease in tumor weight after paclitaxel treatment compared to nontar-

geting control siRNA-DOPC treated with paclitaxel (p = 0.008 and 0.005 for SKOv3ip and HeyA8 models, respectively; t test; Figures 8G and 8H). Depletion of *SIK2,* independent from
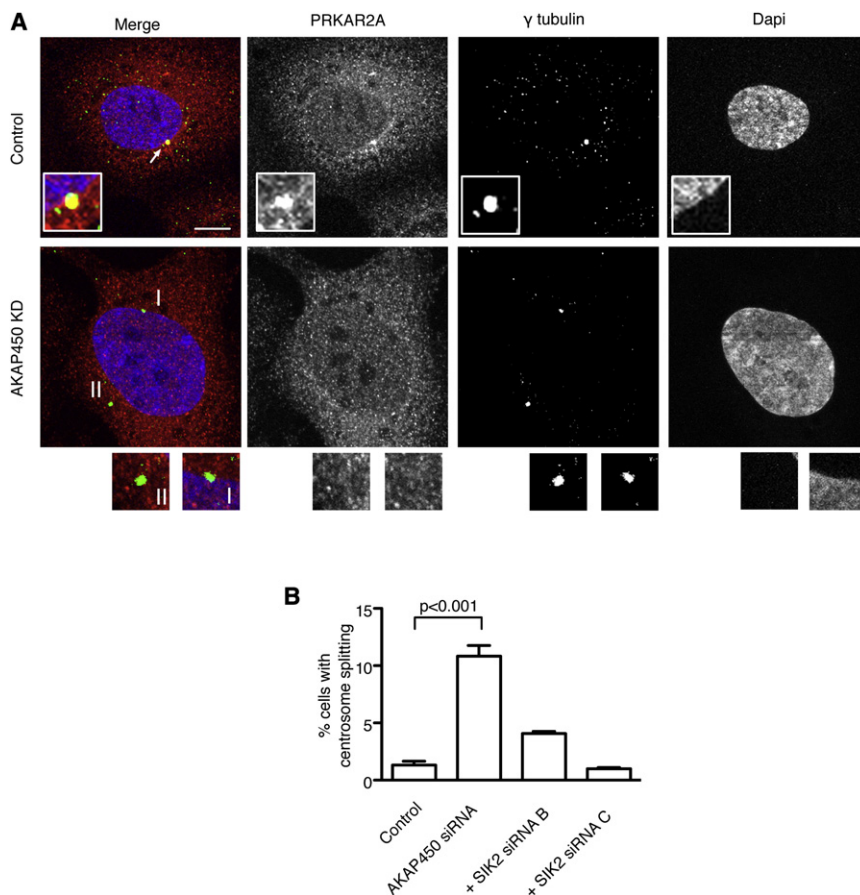
Figure 6. Centrosome Localization of PRKAR2A Is Required for Regulating the Appropriate Timing of Centrosome Separation by SIK2

(A) SKOv3 cells were transfected with the indicated siRNAs for 72 hr, then fixed and stained. The centrosome expression of PRKAR2A is present in control cells (arrow) but absent after KD of AKAP450 (I and II).

(B) Bar plots represent the mean ± SD of triplicate percentages of cells with CS after transfection with the indicated siRNAs. Depletion of AKAP450 resulted in a significant increase in CS, whereas codepletion of AKAP450 and SIK2 rescued this phenotype.

Scale bar represents 5 μm. See also Figure S6.

paclitaxel, resulted in a modest decrease in tumor weight in the SKOv3ip model (p = 0.2) and a modest but significant decrease of tumor weights in the HeyA8 model (p = 0.02). Taken together, these results confirm the effect of loss of *SIK2* in inducing synergy to paclitaxel in vitro and in vivo.

DISCUSSION

We have previously shown that LKB1, a master kinase for all members of the AMPK superfamily, plays an important role in regulating mitosis through mechanisms that remained unclear (Bettencourt-Dias et al., 2004). In this work, we believe we have identified a previously unrecognized role for SIK2, a member of the AMPK family in regulating centrosome separation during mitosis. The effect of depletion of *SIK2* on mitosis and centrosome function is unlikely to be secondary to depletion of energy reserves. Previous work has shown that the key role that SIK2 plays in metabolism is in regulating energy balance in refeeding from starvation (Dentin et al., 2007; Ryu et al., 2009; Wang et al., 2008). During fasting ATP depletion leads to PKA activation that inhibits SIK2 resulting in dephosphorylation of its cytoplasmic target TORC2 and its accumulation in the nucleus. Nuclear TORC2 enhances CREB-mediated gluconeogenesis in an effort to increase ATP production to maintain its intracellular level. On refeeding from starvation, rising ATP levels lead to inactivation of PKA and this results in SIK2 activation

leading to phosphorylation of TORC2 and its cytoplasmic retention and degradation. This results in inhibition of gluconeogenesis and decreased ATP production through this pathway. Thus, based on this evidence depletion of SIK2 would not be expected to lead to loss of intracellular ATP under normal feeding conditions. Indeed, work in *Drosophila* has shown that depletion of the ortholog of SIK2 results in enhanced resistance to metabolic stress in neurons (Wang et al., 2008). We have also shown here that depletion of SIK2 did not result in decreased ATP levels in SKOv3 cells. Therefore, loss of ATP cannot explain the mitotic phenotypes that we have observed after *SIK2* depletion.

We propose that displacement of PRKAR2A from the centrosome in prophase relieves SIK2 from inhibition. This molecular event coupled with higher centrosome expression of SIK2 at the onset of mitosis may initiate centrosome separation by inducing additional phosphorylation of centrosome linker proteins such as C-Nap1. We speculate that NEK2 may induce subthreshold phosphorylation of C-Nap1 and that optimal phosphorylation is achieved at the onset of mitosis by the activity of SIK2. These molecular events could complement the known decrease in phosphatases, such as PP1α, that oppose NEK2 activity before the onset of mitosis (Meraldi and Nigg, 2001). Our findings add further proof to the emerging evidence of coupling cancer cell metabolism and mitosis functions of the AMPK family members.

It is important to note that SIK2 is a rare example of a therapeutic target that on depletion results in mitosis-dependent synergy with paclitaxel as well as G1/S arrest and decreased cancer growth independent from taxanes. It is becoming clearer that regimens involving combination therapies targeting different phases of the cell cycle are desirable for optimal cancer response. Several microtubule-independent mitotic inhibitors have been tested in early clinical trials with or without taxanes. The results from these trials are still emerging but such approaches have so far resulted in disease stabilization or partial
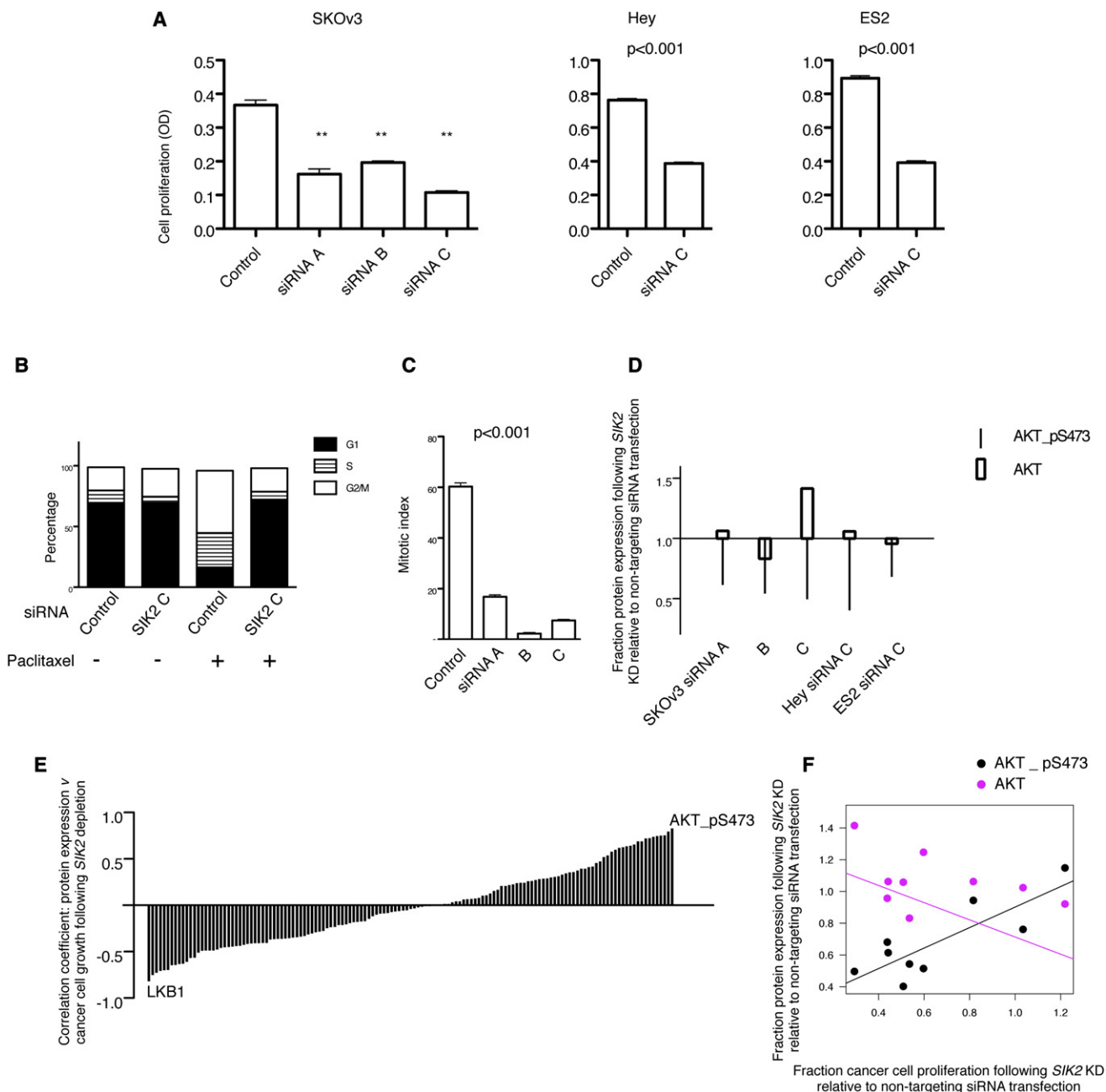
Figure 7. SIK2 Is Required for AKT Phosphorylation and Growth of Ovarian Cancer Cells

(A) SKOv3, ES2, and Hey cells were either transfected using nontargeting control siRNA or the indicated *SIK2* siRNAs for 5 days. Cells were fixed and stained using crystal violet. Shown is the mean ± SEM of 12 replicate values per siRNA transfection type from two independent experiments in SKOv3 cells. **p < 0.001. Error bars for Hey and ES2 cells represent the SEM of six replicate values per siRNA transfection type from two independent experiments.

(B) Typical cell-cycle distributions are presented after transfection of SKOv3 cells with the indicated siRNAs.

(C) Cells were transfected using the indicated siRNA for 48 hr then treated with paclitaxel 100 nM for 24 hr, fixed, and stained using antiphosphohistone H3 antibody to calculate the mitotic index (MI) using flow cytometry. Shown is the mean MI (±SD) of two independent experiments.

(D) Cell lines were transfected with the indicated *SIK2* siRNAs and control nontargeting siRNAs for 48 hr, then harvested for analysis of protein expression using reverse phase protein arrays. Shown is the fraction of expression of AKT-pS437 and total AKT after *SIK2* siRNA transfection relative to protein expression after nontargeting siRNAs.

(E) The expression of 139 proteins (Table S4) was estimated using reverse phase protein arrays as in (D) after transfection of cancer cells using three *SIK2* siRNAs and one nontargeting control in three cell lines: SKOv3, Hey, and ES2. The expression of each of the 139 proteins was correlated with cancer cell growth that was measured in (A). Each bar represents the coefficient of the correlation between the expression of each of the proteins in nine cell lines (3 *SIK2* siRNAs × 3 cell lines) and the growth of the cancer cell line from which the protein was measured. Positive values indicate that higher expression of a protein correlates with more cancer cell growth. Negative values indicate that higher expression correlate with poor growth.
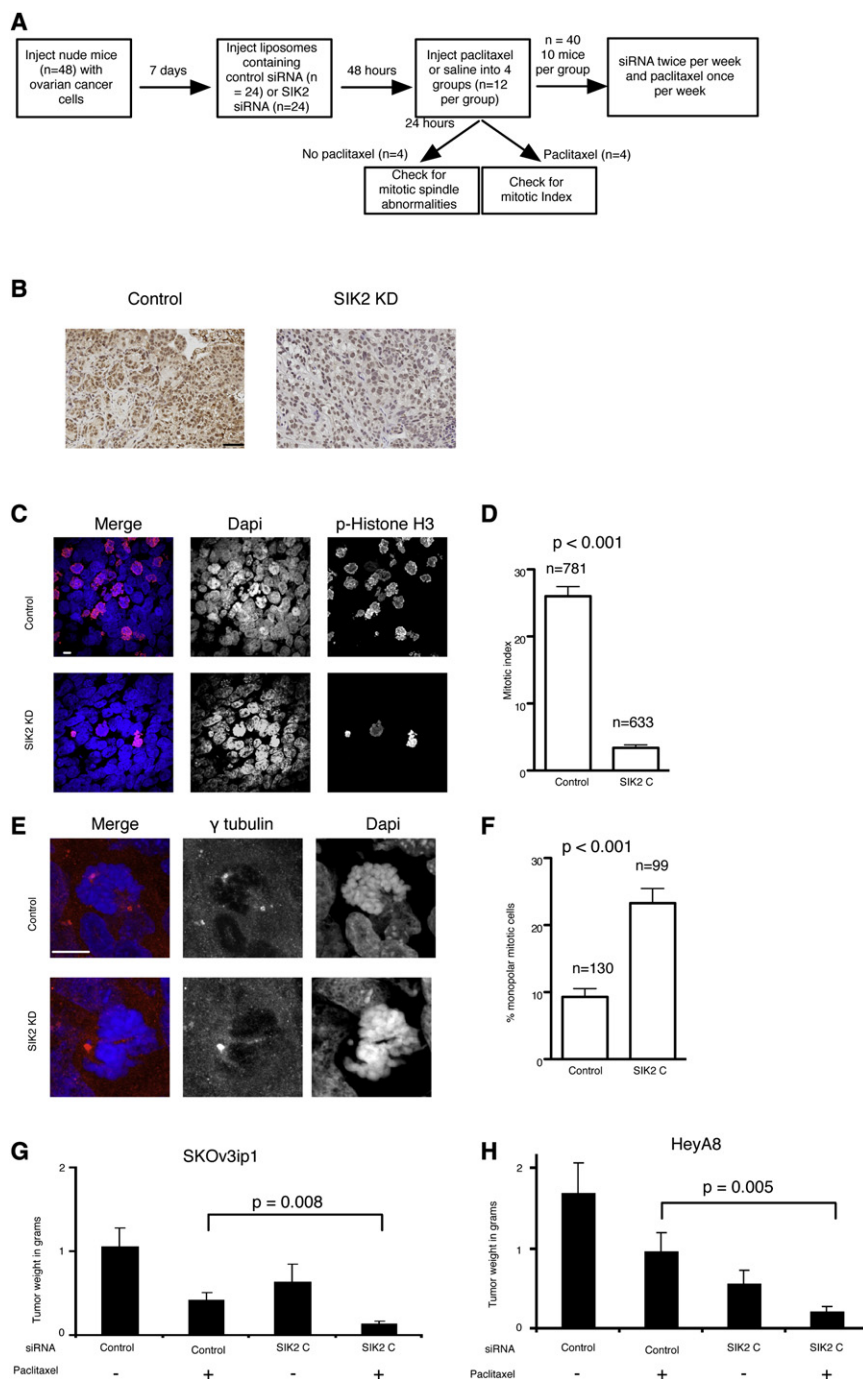
Figure 8. Loss of *SIK2* Sensitizes Ovarian Cancer Cells to Paclitaxel In Vivo

(A) A flow diagram showing the design of the in vivo experiment.

(B) Immunohistochemical confirmation of SIK2 depletion in SKOv3ip1 tissue sections using anti-SIK2 antibody. Scale bar represents 50 μm.

(C–F) Tumor sections (5 μm) were stained using the indicated antibodies. (C and D) Sections were stained using the indicated antibodies to calculate the mitotic index per field by manually counting phospho-Histone H3 positive nuclei and total number of nuclei. Shown in (C) is the mean ± SEM of the MIs from seven fields from two mice. In (E), an example of monopolar centrosome orientation after *SIK2* KD in mice is shown. (F) Bar plot representation of the mean ± SEM of the percentage of mitotics with monopolar centrosome orientation from two mice (two slides per mouse).

(G and H) Mean tumor weights (±SD) obtained from 10 mice per siRNA type in SKOv3 cells and Hey cells. Scale bar represents 10 μm.

S473 and this may contribute to the delayed cell-cycle progression. Another possible contributing factor is the centrosome abnormalities after *SIK2* depletion in interphase. It is well documented that the centrosome functions as a docking site for several proteins involved in cell-cycle progression (Matsumoto and Maller, 2004). Centrosome dysfunction after loss of key centrosome proteins or centrosome displacement results in severe G1 arrest (Hinchcliffe et al., 2001; Keryer et al., 2003; Khodjakov and Rieder, 2001; Matsumoto and Maller, 2004). We have shown that loss of *SIK2* results in profound abnormalities in centrosome position, and function that may be the underlying cause for the observed G1 arrest.

An important consideration for examining the potential therapeutic role of SIK2 will be to test the toxicity profile after its inhibition. This could be achieved in mouse models of ovarian cancer metastasis using SIK2 inhibitors. To our knowledge, no specific inhibitors for SIK2 are currently available. Future work focusing on resolving the structure of SIK2 to inform the development of inhibitors in parallel with running small-molecule inhibitor compound screens will be important to identify prototype inhibitors of SIK2. The work shown here provides extensive phenotypic and biochemical data to support the development of

responses (Blagden et al., 2008; Gautschi et al., 2008; Perez de Castro et al., 2008; Strebhardt and Ullrich, 2006). Targeting SIK2 may offer inhibition of cancer cell growth by targeting multiple phases of the cell cycle. Using reverse phase protein arrays we showed that SIK2 is required for phosphorylation of AKT at

(F) Shown are the regression lines for the correlation between the fraction of ovarian cancer cell proliferation after *SIK2* depletion relative to nontargeting control and the fraction expression of AKT-pS437 or total AKT after *SIK2* depletion relative to nontargeting controls.
See also Figure S7 and Table S4.

SIK2 inhibitors. Such inhibitors will be highly valuable for further testing of the biological and therapeutic potential of SIK2 and for examining its toxicity profile in vivo. It is important to consider that in mammals SIK2 plays a role in regulating energy balance in subcutaneous fat on refeeding from starvation. However, its role in maintaining energy reserves under normal feeding conditions remains unclear. Therefore, whether its inhibition under normal feeding conditions will result in energy imbalance and consequent toxicities remains to be tested in animal models.

In this work we showed that the expression level of *SIK2* correlated with prognosis in patients with ovarian high-grade serous cancers and with paclitaxel response. In addition we showed that the expression level of *SIK2* did not correlate with carboplatin response in the context of a prospective randomized study. Furthermore, our data in vitro and in xenograft models show a clear relationship between the intracellular levels of *SIK2* and response to paclitaxel. However, this work does not exclude the possibility of an effect of SIK2 on response to non anti-tubulin agents. It will be interesting to investigate the effect of SIK2 on response to other chemotherapeutic agents in vitro and in clinical samples in future studies. Regulation of *SIK2* might also potentiate targeted therapies. Knockdown of *SIK2* was shown to inhibit phosphorylation and activation of AKT that might be put to use in overcoming paradoxical activation of AKT by partial mTOR inhibitors such as rapamycin (O'Reilly et al., 2006).

In summary, we believe this work identifies a previously unrecognized role of SIK2 in regulating cell-cycle progression and suggests SIK2 as an attractive target for treatment in a proportion of ovarian cancers that overexpress this protein.

EXPERIMENTAL PROCEDURES

Automated Image Acquisition, Segmentation, and Analysis
Automated image acquisition and analysis were performed using the In Cell Analyzer 1000 and the In Cell investigator software, respectively (GE Healthcare).

The Australian Ovarian Cancer Study
This was a population-based, multicenter translational study that comprised prospective collection of biospecimens, clinical, and epidemiological data from patients with primary epithelial ovarian, primary peritoneal, and fallopian tube cancer diagnosed between 2001 and 2005. All patients were prospectively consented using a protocol approved by human research ethics committees at multiple participating clinical and research centers. Further details of the AOCS cohort can be found at http://www.aocstudy.org and in the Supplementary Experimental Procedures.

In Vivo Experiments in Mice
All mouse experiments were approved by the Institutional Animal Care and Use Committee of the University of Texas MD Anderson Cancer Center. Mice were cared for in accordance with guidelines set forth by the American Association for Accreditation of Laboratory Animal Care and the U.S. Public Health Service Policy on Human Care and Use of Laboratory Animals. Female nude mice were inoculated with ovarian cancer cell lines (HeyA8 or SKOV3ip1) into the peritoneal cavity. After 1 week, SiRNA was incorporated in DOPC-nanoliposomes and administered intraperitoneally (IP) at a dose of 150 μg/kg per mouse, biweekly. Paclitaxel was administered IP once a week at a dose of 100 μg per mouse for HeyA8 and 75 μg per mouse for SKOV3ip1. Mice were treated for 3 to 4 weeks and all treatment groups were sacrificed and necropsied when any single group became moribund and assayed for tumor weight.

Detailed additional methods are available as Supplemental Information.

REFERENCES

Ahmed, A.A., Mills, A.D., Ibrahim, A.E., Temple, J., Blenkiron, C., Vias, M., Massie, C.E., Iyer, N.G., McGeoch, A., Crawford, R., et al. (2007). The extracellular matrix protein TGFBI induces microtubule stabilization and sensitizes ovarian cancers to paclitaxel. Cancer Cell *12*, 514–527.

Bekier, M.E., Fischbach, R., Lee, J., and Taylor, W.R. (2009). Length of mitotic arrest induced by microtubule-stabilizing drugs determines cell death after mitotic exit. Mol. Cancer Ther. *8*, 1646–1654.

Bettencourt-Dias, M., Giet, R., Sinka, R., Mazumdar, A., Lock, W.G., Balloux, F., Zafiropoulos, P.J., Yamaguchi, S., Winter, S., Carthew, R.W., et al. (2004). Genome-wide survey of protein kinases required for cell cycle progression. Nature *432*, 980–987.

Blagden, S.P., Molife, L.R., Seebaran, A., Payne, M., Reid, A.H., Protheroe, A.S., Vasist, L.S., Williams, D.D., Bowen, C., Kathman, S.J., et al. (2008). A phase I trial of ispinesib, a kinesin spindle protein inhibitor, with docetaxel in patients with advanced solid tumors. Br. J. Cancer *98*, 894–899.

Carlson, C.R., Witczak, O., Vossebein, L., Labbe, J.C., Skalhegg, B.S., Keryer, G., Herberg, F.W., Collas, P., and Tasken, K. (2001). CDK1-mediated phosphorylation of the RIIalpha regulatory subunit of PKA works as a molecular switch that promotes dissociation of RIIalpha from centrosomes at mitosis. J. Cell Sci. *114*, 3243–3254.

Dentin, R., Liu, Y., Koo, S.H., Hedrick, S., Vargas, T., Heredia, J., Yates, J., 3rd, and Montminy, M. (2007). Insulin modulates gluconeogenesis by inhibition of the coactivator TORC2. Nature *449*, 366–369.

Fry, A.M., Mayor, T., Meraldi, P., Stierhof, Y.D., Tanaka, K., and Nigg, E.A. (1998a). C-Nap1, a novel centrosomal coiled-coil protein and candidate substrate of the cell cycle-regulated protein kinase Nek2. J. Cell Biol. *141*, 1563–1574.

Fry, A.M., Meraldi, P., and Nigg, E.A. (1998b). A centrosomal function for the human Nek2 protein kinase, a member of the NIMA family of cell cycle regulators. EMBO J. *17*, 470–481.

Gautschi, O., Heighway, J., Mack, P.C., Purnell, P.R., Lara, P.N., Jr., and Gandara, D.R. (2008). Aurora kinases as anticancer drug targets. Clin. Cancer Res. *14*, 1639–1648.

Hinchcliffe, E.H., Miller, F.J., Cham, M., Khodjakov, A., and Sluder, G. (2001). Requirement of a centrosomal activity for cell cycle progression through G1 into S phase. Science *291*, 1547–1550.

Huang, H.C., Shi, J., Orth, J.D., and Mitchison, T.J. (2009). Evidence that mitotic exit is a better cancer therapeutic target than spindle assembly. Cancer Cell *16*, 347–358.

Katoh, Y., Takemori, H., Horike, N., Doi, J., Muraoka, M., Min, L., and Okamoto, M. (2004). Salt-inducible kinase (SIK) isoforms: their involvement in steroidogenesis and adipogenesis. Mol. Cell. Endocrinol. *217*, 109–112.

Katoh, Y., Takemori, H., Lin, X.Z., Tamura, M., Muraoka, M., Satoh, T., Tsuchiya, Y., Min, L., Doi, J., Miyauchi, A., et al. (2006). Silencing the constitutive active transcription factor CREB by the LKB1-SIK signaling cascade. FEBS J. *273*, 2730–2748.

Keryer, G., Witczak, O., Delouvee, A., Kemmner, W.A., Rouillard, D., Tasken, K., and Bornens, M. (2003). Dissociating the centrosomal matrix protein AKAP450 from centrioles impairs centriole duplication and cell cycle progression. Mol. Biol. Cell *14*, 2436–2446.

Khodjakov, A., and Rieder, C.L. (2001). Centrosomes enhance the fidelity of cytokinesis in vertebrates and are required for cell cycle progression. J. Cell Biol. *153*, 237–242.

Landsverk, H.B., Carlson, C.R., Steen, R.L., Vossebein, L., Herberg, F.W., Tasken, K., and Collas, P. (2001). Regulation of anchoring of the RIIalpha regulatory subunit of PKA to AKAP95 by threonine phosphorylation of RIIalpha: implications for chromosome dynamics at mitosis. J. Cell Sci. *114*, 3255–3264.

Lin, Y.G., Immaneni, A., Merritt, W.M., Mangala, L.S., Kim, S.W., Shahzad, M.M., Tsang, Y.T., Armaiz-Pena, G.N., Lu, C., Kamat, A.A., et al. (2008). Targeting aurora kinase with MK-0457 inhibits ovarian cancer growth. Clin. Cancer Res. *14*, 5437–5446.

Martin, M., Rodriguez-Lescure, A., Ruiz, A., Alba, E., Calvo, L., Ruiz-Borrego, M., Munarriz, B., Rodriguez, C.A., Crespo, C., de Alava, E., et al. (2008). Randomized phase 3 trial of fluorouracil, epirubicin, and cyclophosphamide alone or followed by Paclitaxel for early breast cancer. J. Natl. Cancer Inst. *100*, 805–814.

Matsumoto, Y., and Maller, J.L. (2004). A centrosomal localization signal in cyclin E required for Cdk2-independent S phase entry. Science *306*, 885–888.

Mayer, T.U., Kapoor, T.M., Haggarty, S.J., King, R.W., Schreiber, S.L., and Mitchison, T.J. (1999). Small molecule inhibitor of mitotic spindle bipolarity identified in a phenotype-based screen. Science *286*, 971–974.

Mayor, T., Hacker, U., Stierhof, Y.D., and Nigg, E.A. (2002). The mechanism regulating the dissociation of the centrosomal protein C-Nap1 from mitotic spindle poles. J. Cell Sci. *115*, 3275–3284.

McGuire, W.P., Hoskins, W.J., Brady, M.F., Kucera, P.R., Partridge, E.E., Look, K.Y., Clarke-Pearson, D.L., and Davidson, M. (1996). Cyclophosphamide and cisplatin compared with paclitaxel and cisplatin in patients with stage III and stage IV ovarian cancer. N. Engl. J. Med. *334*, 1–6.

Meraldi, P., and Nigg, E.A. (2001). Centrosome cohesion is regulated by a balance of kinase and phosphatase activities. J. Cell Sci. *114*, 3749–3757.

Monks, A., Scudiero, D., Skehan, P., Shoemaker, R., Paull, K., Vistica, D., Hose, C., Langley, J., Cronise, P., Vaigro-Wolff, A., et al. (1991). Feasibility of a high-flux anticancer drug screen using a diverse panel of cultured human tumor cell lines. J. Natl. Cancer Inst. *83*, 757–766.

O'Reilly, K.E., Rojo, F., She, Q.B., Solit, D., Mills, G.B., Smith, D., Lane, H., Hofmann, F., Hicklin, D.J., Ludwig, D.L., et al. (2006). mTOR inhibition induces upstream receptor tyrosine kinase signaling and activates Akt. Cancer Res. *66*, 1500–1508.

Perez de Castro, I., de Carcer, G., Montoya, G., and Malumbres, M. (2008). Emerging cancer therapeutic opportunities by inhibiting mitotic kinases. Curr. Opin. Pharmacol. *8*, 375–383.

Ryu, D., Oh, K.J., Jo, H.Y., Hedrick, S., Kim, Y.N., Hwang, Y.J., Park, T.S., Han, J.S., Choi, C.S., Montminy, M., and Koo, S.H. (2009). TORC2 regulates hepatic insulin signaling via a mammalian phosphatidic acid phosphatase, LIPIN1. Cell Metab. *9*, 240–251.

Screaton, R.A., Conkright, M.D., Katoh, Y., Best, J.L., Canettieri, G., Jeffries, S., Guzman, E., Niessen, S., Yates, J.R., 3rd, Takemori, H., et al. (2004). The CREB coactivator TORC2 functions as a calcium- and cAMP-sensitive coincidence detector. Cell *119*, 61–74.

Strebhardt, K., and Ullrich, A. (2006). Targeting polo-like kinase 1 for cancer therapy. Nat. Rev. Cancer *6*, 321–330.

Tothill, R.W., Tinker, A.V., George, J., Brown, R., Fox, S.B., Lade, S., Johnson, D.S., Trivett, M.K., Etemadmoghadam, D., Locandro, B., et al. (2008). Novel molecular subtypes of serous and endometrioid ovarian cancer linked to clinical outcome. Clin. Cancer Res. *14*, 5198–5208.

Tsou, M.F., and Stearns, T. (2006). Mechanism limiting centrosome duplication to once per cell cycle. Nature *442*, 947–951.

Wang, B., Goode, J., Best, J., Meltzer, J., Schilman, P.E., Chen, J., Garza, D., Thomas, J.B., and Montminy, M. (2008). The insulin-regulated CREB coactivator TORC promotes stress resistance in Drosophila. Cell Metab. *7*, 434–444.